Applied Physics Express 7, 035502 (2014)
http://dx.doi.org/10.7567/APEX.7.035502

Phase separation of thick (~1 μm) $In_xGa_{1-x}N$ ($x \sim 0.3$) grown on AlN/Si(111): Simultaneous emergence of metallic In–Ga and GaN-rich InGaN

Akio Yamamoto[1,2], Md. Tanvir Hasan[1,2], Akihiro Mihara[1,2], Norihiko Narita[3], Naoteru Shigekawa[4], and Masaki Kuzuhara[1]

[1]*University of Fukui, Fukui 910-8507, Japan*
[2]*JST-CREST, Chiyoda, Tokyo 102-0076, Japan*
[3]*The Kansai Electric Power Co., Inc., Amagasaki, Hyogo 661-0974, Japan*
[4]*Osaka City University, Osaka 558-8585, Japan*

Received January 6, 2014; accepted January 21, 2014; published online February 6, 2014

0.3–2-μm-thick $In_xGa_{1-x}N$ ($x \sim 0.3$) films are grown at 650 °C on AlN/Si(111) substrates by metal organic vapor phase epitaxy. When the thickness of an epitaxial InGaN film exceeds ~1 μm, peaks of GaN-rich InGaN(0002) and metallic In(101) appear in the X-ray diffraction profiles. The InN composition ~0.03 in the GaN-rich InGaN film is in agreement with the solubility of InN in GaN at 650 °C. The metallic In contains a small amount (~0.03 at. %) of Ga. These results clearly show that the epitaxial InGaN film is phase-separated into GaN-rich and InN-rich InGaN. The latter is changed into metallic In–Ga owing to its thermal instability at 650 °C.

Direct-band-gap InGaN alloys have proven to be important materials because of their unique property of wide spectral tunability, which can be adjusted continuously from the ultraviolet region to the infrared region. This tunability offers many possibilities in a variety of device applications, including high-brightness visible-light-emitting diodes, lasers, and full-spectrum multijunction solar cells. Very thin InGaN layers in the form of single or multiple quantum wells have been widely used as active layers in LED, LD, and photovoltaic devices.[1–3] Thick (bulk) InGaN layers are also promising for homojunction InGaN solar cells.[3]

In almost all the cases, InGaN alloys have been prepared by metal organic vapor phase epitaxy (MOVPE) or molecular beam epitaxy (MBE), where growth proceeds under conditions far from the thermal equilibrium. Ho and Stringfellow[4] have theoretically shown that the large difference in interatomic spacing between GaN and InN gives rise to a solid-phase miscibility gap. Despite the prediction, single-phase InGaN films with a wide range of InN compositions have been grown by MBE and MOVPE. However, it should be pointed out that films grown by MBE or MOVPE under nonequilibrium conditions are essentially unstable because they are kept in a "frozen" state and, therefore, show a tendency towards clustering and/or decomposition so that the system reaches an energetically stable state. The rate of decomposition can be determined on the basis of the solid-state diffusion mobility of atoms. The stability of InGaN at room temperature is very high because the diffusion mobility of atoms is negligibly low at room temperature. As the film temperature increases, on the other hand, the rates of decomposition should be increased and phase separation should occur.

There have been so many reports on the decomposition and/or phase separation of InGaN during and after growth. Many groups[5–8] have reported thermal damage, phase separation, or metallic In formation in InGaN/GaN quantum wells. Such phenomena have been found to occur mainly when a p-type GaN layer is grown at a temperature higher than that for the InGaN-well layer. Phase separation in bulk InGaN has also been extensively studied.[9–15] According to the phase diagram of InGaN proposed by Ho and Stringfellow,[4] spinodal decomposition should result in the simultaneous formation of InN-rich InGaN and GaN-rich InGaN, as discussed by Doppalapudi et al.[12] However, Doppalapudi et al.[12] did not find such simultaneous formation of the two phases. They found only InN-rich $In_xGa_{1-x}N$ ($x \sim 0.97$) in an as-grown $In_{0.35}Ga_{0.65}N$ film, while only GaN-rich InGaN ($2\theta \sim 34.5°$) was observed after the annealing of the film at 675 °C. Pantha et al.[13] have studied the details of the phase separation of $In_{0.65}Ga_{0.35}N$ films grown at 610 °C by MOVPE. They have shown that there is a maximum thickness of $In_{0.65}Ga_{0.35}N$ that can be grown without phase separation, which is markedly dependent on growth rate. However, the formation of InN-rich InGaN and/or GaN-rich InGaN has not been reported. Thus, phase separation of InGaN has not yet been completely understood, despite the many studies.

In this paper, we report on the simultaneous formation of metallic In–Ga and GaN-rich InGaN during the MOVPE growth of $In_xGa_{1-x}N$ ($x \sim 0.3$) at 650 °C. It is found that the simultaneous emergence of metallic In–Ga and GaN-rich InGaN is accompanied by the consumption of epitaxial $In_xGa_{1-x}N$ ($x \sim 0.3$). Considering the thermal instability of InN-rich InGaN, it is reasonable to conclude that metallic In–Ga is formed through InN-rich InGaN. These findings clearly show that $In_xGa_{1-x}N$ ($x \sim 0.3$) is phase-separated into InN-rich InGaN and GaN-rich InGaN, as predicted by Ho and Stringfellow.[4] The annealing of the sample in NH_3 flow at 650 °C is found to markedly enhance the decomposition reaction. This suggests the contribution of hydrogen, which is generated through the decomposition of NH_3, to the decomposition reaction. The decomposition reaction is almost suppressed by reducing the growth temperature to 570 °C. It should be pointed out that the use of the AlN/Si(111) substrate enables us to clearly observe such phase separation. The use of a GaN-free substrate and/or buffer is indispensable for detecting GaN-rich InGaN as a product of phase separation by X-ray diffraction (XRD), since the InN content in the GaN-rich InGaN is very small (~0.03).

The growth of $In_xGa_{1-x}N$ alloys ($x \sim 0.3$) was conducted using an MOVPE system. Si(111) wafers with a layer of separately MOVPE-grown AlN (100 nm thick) were used as the starting substrates. During the growth process, the substrates were first annealed at 950 °C in NH_3, after which the temperature was ramped down to the growth temperature (550–700 °C). Triethylgallium (TEG), trimethylindium (TMI), and ammonia (NH_3) were used as Ga, In, and N sources, respectively. The growth pressure was fixed at 150 Torr. The growth rate of InGaN was about 0.7 μm/h, and films of 0.5–2 μm thicknesses were prepared. The structures of the

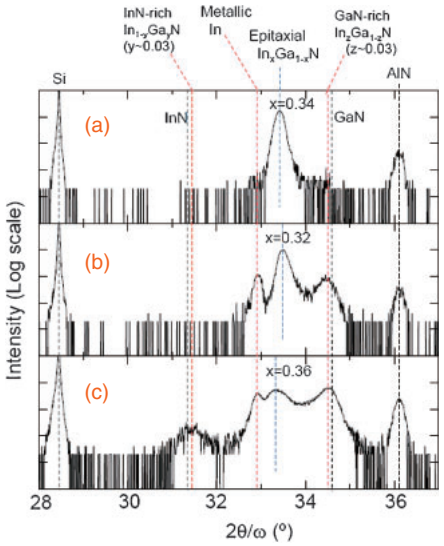

Fig. 1. XRD $2\theta/\omega$ profiles for epitaxial $In_xGa_{1-x}N$ ($x = 0.32$–0.36) grown at 650 °C with a different thickness (different growth time). (a) Thickness: 0.7 μm (growth time: 60 min), (b) thickness: 1.1 μm (growth time: 90 min), (c) thickness: 1.8 μm (growth time: 140 min).

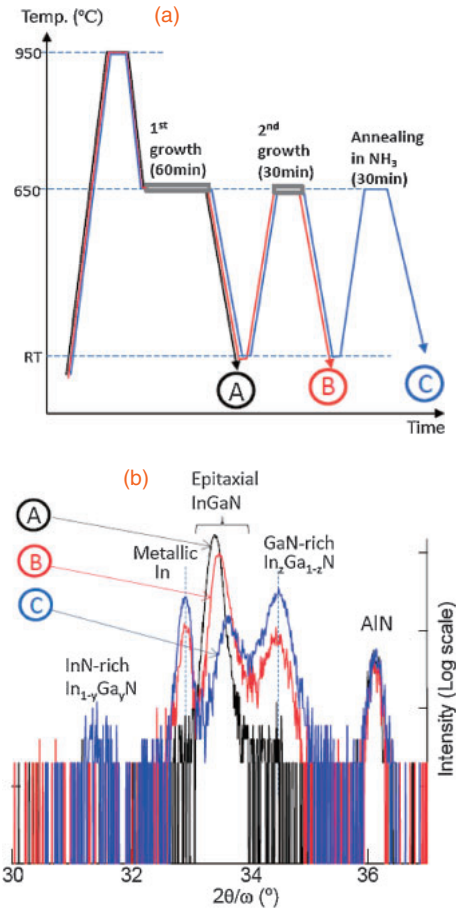

Fig. 2. Time chart of the preparation for three different samples A, B, and C (a), and XRD $2\theta/\omega$ profiles for the three samples (b). See text for details of sample preparation.

films were characterized by XRD and field-emission scanning electron microscopy (FESEM) measurements. The InN or GaN compositions of the grown films were determined from the XRD $2\theta/\omega$ patterns on the basis of Vegard's law, assuming that the films are fully relaxed. Energy dispersion spectra (EDS) in the FESEM system were also used to measure the compositions of metal droplets formed on the sample surface.

First, the effects of InGaN film thickness on XRD profiles are discussed. Figure 1 shows the XRD $2\theta/\omega$ patterns for the epitaxial $In_xGa_{1-x}N$ ($x = 0.32$–0.36) grown at 650 °C with a different thickness (different growth time). The result for a 0.7-μm-thick sample (growth time: 60 min) is shown in Fig. 1(a). One can see that a single peak corresponding to a single-phase $In_xGa_{1-x}N$ ($x = 0.34$) is observed together with the Si(111) and AlN(0002) peaks. When the film thickness was increased to 1.1 μm (growth time: 90 min) under the same growth conditions as the case for Fig. 1(a), two new peaks appeared, as shown in Fig. 1(b), indicating the occurrence of phase separation. These new peaks at $2\theta \sim 32.9°$ and $2\theta \sim 34.5°$ are very close to those for metallic In(101) and GaN(0002), respectively. Note that the InN content in the epitaxial $In_xGa_{1-x}N$ was decreased from 0.34 to 0.32 when the growth time was increased from 60 to 90 min. Figure 1(c) shows the result for a sample of 1.8 μm thickness, which was grown with a high TMI molar ratio in the vapor to obtain a high-InN-content sample. The two peaks at $2\theta \sim 32.9°$ and $2\theta \sim 34.5°$ became much stronger than those for the epitaxial $In_xGa_{1-x}N$. Note that the positions of the two peaks at $2\theta \sim 32.9°$ and $2\theta \sim 34.5°$ were unchanged despite the higher InN content in the epitaxial $In_xGa_{1-x}N$. In this case, a new peak very close to InN(0002) appeared at $2\theta \sim 31.5°$ additionally. Although the peaks at $2\theta \sim 31.5°$ and $2\theta \sim 34.5°$ are very close to the InN(0002) and GaN(0002) peaks, respectively, they are not due to pure InN and GaN. Therefore, they are denoted as InN-rich $In_{1-y}Ga_yN(0002)$ and GaN-rich $In_zGa_{1-z}N(0002)$. By the precise measurement of the lattice constant by XRD, y and z were determined to be 0.02–0.03 and 0.02–0.05, respectively.

As described above, the epitaxial $In_xGa_{1-x}N$ ($x = 0.3$–0.4) was found to show phase separation when the thickness exceeded approximately 1 μm. The following experiments were conducted to further investigate the process of phase separation. Three different samples were prepared through the process shown in Fig. 2(a). After the annealing of AlN/Si wafers at 950 °C in NH_3, an $In_xGa_{1-x}N$ ($x = 0.34$) layer was deposited for 60 min (1st InGaN growth) on three wafers. After cooling the wafers to RT, one of them (Sample A) was taken out of the MOVPE system to measure the XRD $2\theta/\omega$ profiles. After evacuating the growth chamber and heating the remaining two wafers, the second $In_xGa_{1-x}N$ growth was performed for 30 min at 650 °C. Again, one of the two wafers (Sample B) was taken out of the MOVPE system after the cooling. Finally, the remaining wafer was annealed at 650 °C in NH_3 for 30 min (Sample C). XRD $2\theta/\omega$ profiles for these three samples are compared in Fig. 2(b). From the results, one can see that, as the process proceeds from the 1st growth to the final annealing in NH_3, the diffraction intensity for the epitaxial $In_xGa_{1-x}N$ peak markedly decreases and the InN composition x is also reduced. In conjunction with these changes, the GaN-rich $In_zGa_{1-z}N(0002)$ and the peak at $2\theta \sim 32.9°$ became strong coincidently. It is pointed out that the diffraction intensity of the epitaxial $In_xGa_{1-x}N$ is lower in Sample B than in Sample A, despite the additional 30 min

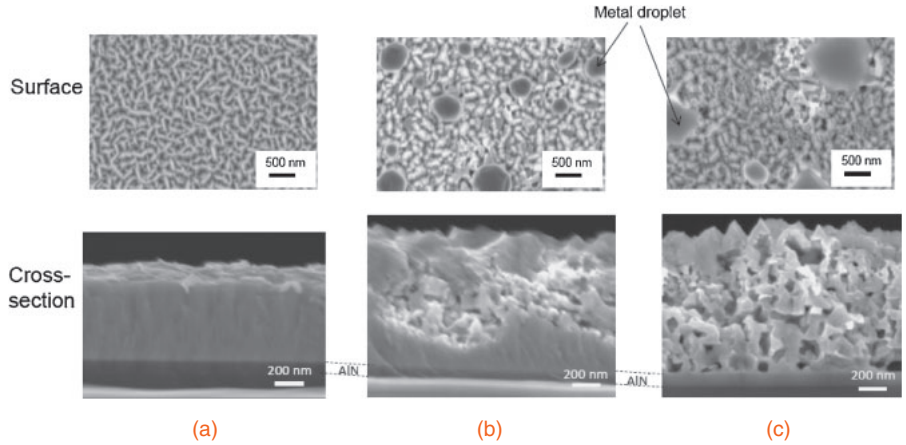

Fig. 3. FESEM images of surfaces and cross sections for Samples A (a), B (b), and C (c), shown in Fig. 2.

growth. The reduction in diffraction intensity was more marked after the annealing in NH_3 (Sample C). The results shown in Fig. 2(b) clearly reveal that the epitaxial $In_xGa_{1-x}N$ is consumed to form the GaN-rich $In_zGa_{1-z}N$ and metallic In. As seen in Figs. 1 and 2(b), the InN-rich $In_{1-y}Ga_yN(0002)$ peak appeared occasionally, but not always. This seems to show that the InN-rich $In_{1-y}Ga_yN$ is unstable. Therefore, it is speculated that the InN-rich $In_{1-y}Ga_yN$ changes swiftly into metallic $In_{1-y}Ga_y$. This is supported by the finding that InN is very unstable and easily decomposed at 650 °C.[16] This speculation indicates that metallic In should contain a small amount of Ga. As discussed later, it was found that In droplets formed on the film surface contain a small amount of Ga (~3 at. %). Therefore, the peak at $2\theta \sim 32.9°$ is due to metallic $In_{1-y}Ga_y$ ($y \sim 0.03$). From the phase diagram of InGaN predicted by Ho and Stringfellow,[4] the spinodal decomposition should result in the simultaneous formation of InN-rich InGaN and GaN-rich InGaN, as discussed by Doppalapudi et al.[12] The compositions in InN-rich InGaN and GaN-rich InGaN should be determined by the solubility of GaN in InN and that of InN in GaN. They were reported to be 0.03 and 0.04 at 650 °C, respectively.[4] These values are in good agreement with those obtained in this study ($y = 0.02$–0.03 and $z = 0.02$–0.05).

Figure 3 shows the FESEM images of surfaces and cross sections of Samples A–C. In the case of Sample A, a dense InGaN layer is grown. The corrugated surface feature of the sample is very similar to that for In-polar InN.[17] As shown in Fig. 3(b), many droplets were formed on the surface, and porous regions were formed in the interior of the film after the 90 min growth (60 min for the first growth and 30 min for the second growth). Such metal droplet formation is very similar to the case of the low-pressure-grown InGaN reported by Ho et al.[15] Note that the formation of porous regions is initiated in the middle part of the film, and the dense InGaN layer still remains near the AlN interlayer. This is slightly different from the case for the thermal decomposition of InN,[16] where the formation of porous regions starts near the substrate interface. Since the part nearer to the substrate interface should undergo a longer annealing at 650 °C during growth, it is expected that such a part shows the severest decomposition. As shown in Fig. 3(b), however, the formation of the porous regions is initiated in the middle part of the film. This finding seems to show that a different situation occurs near the interface of the film. For example, stress induced by the substrate might suppress the phase separation of the part near the substrate.[18] This seems to correlate to the presence of a critical thickness of phase separation.[13,19] Compared with Sample A, the film thickness of Sample B increased owing to the prolonged growth time. However, the XRD intensity of epitaxial InGaN is lower than that of Sample A. This is due to the formation of the porous regions. The 30 min annealing in NH_3 flow after the 90 min growth caused marked changes in the film (Sample C). The porous region expanded to the whole part of the film, and the size of the droplets on the surface increased. The shape of voids in the porous region observed in Fig. 3(c) is very similar to those observed in the thermally deteriorated InN at 650 °C.[16] As in the case for InN, nitrogen-terminated planes seem to be selectively attacked. Noted also that, despite the absence of the supply of TMI and TEG in the NH_3 annealing process, the size of metal droplets increased. Therefore, it is reasonable to conclude that materials for forming the droplets are supplied from the interior of the film. From the correspondence between the XRD profiles and the changes in the cross-sectional FESEM view, one can see that the porous parts in the films correspond to the GaN-rich $In_zGa_{1-z}N$. The EDS measurement showed that the metal droplets are composed of about 97 at. % In and 3 at. % Ga. The droplets were removed by dipping samples in a conc. HCl solution. After the HCl etching, the XRD peak at $2\theta \sim 32.9°$ disappeared, indicating that metallic In was scarcely included in the interior of the films. It was also found that the metal droplets were very soft and their shape easily changed mechanically even at room temperature. This finding also indicates that the droplets are not of pure In but an alloy of In and Ga. It is reasonable to consider that metallic In was produced in the interior of the films as a result of phase separation, because porous regions resulting from phase separation are formed at the inner part of the films. The mechanism by which metallic In is pushed out onto the film surface to form droplets is unclear at present. To determine where and how the phase separation of epitaxial $In_xGa_{1-x}N$ initiates is a very interesting issue. It is expected that the decomposition of InGaN initiates at local In-rich InGaN clusters that exist around threading dislocations, as pointed out by Li et al.[8]

Thus, the decomposition of epitaxial $In_xGa_{1-x}N$ into metallic In–Ga and GaN-rich $In_zGa_{1-z}N$ has been clearly

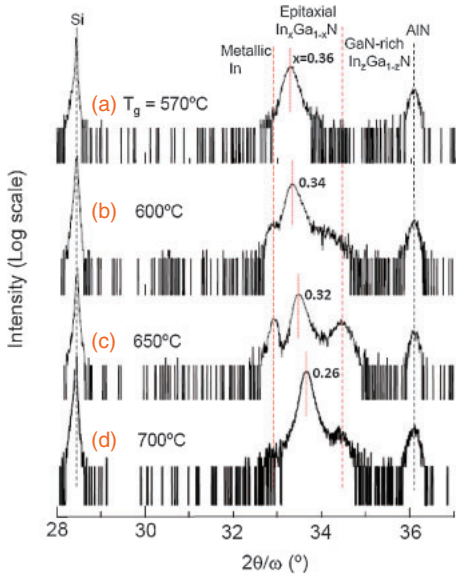

Fig. 4. XRD $2\theta/\omega$ patterns for the epitaxial $In_xGa_{1-x}N$ grown at a different temperature with a constant TMI/(TMI+TEG) molar ratio. Growth time is 90 min for all samples.

shown. From the viewpoint of the application of InGaN, such phase separation needs to be suppressed. The most convenient way to suppress the phase separation may be to reduce growth temperature. Figure 4 shows the XRD $2\theta/\omega$ patterns for the epitaxial $In_xGa_{1-x}N$ grown at a different temperature. One can see that the decomposition reaction is clearly observed near 650 °C. At 700 °C, the peak of In(101) is scarcely observed. This is due to the evaporation of In during growth. Similar XRD profiles have been reported for $In_{0.35}Ga_{0.65}N$ films annealed at approximately 700 °C by Doppalapudi et al.[12] With decreasing growth temperature, phase separation was reduced, and almost suppressed at 570 °C. At 600 °C, the formation of the GaN-rich $In_zGa_{1-z}N$ does not seem to be completed because peaks at $2\theta \sim 34°$ are observed. This is due to the lower diffusion mobility of atoms in InGaN at 600 °C. A longer annealing time will be needed to observe the peak at $2\theta \sim 34.5°$ at approximately 600 °C. Thus, the growth temperature, where two phases of metallic In–Ga and GaN-rich $In_zGa_{1-z}N$ are clearly observed, is limited to a relatively narrow range (<100 °C). From the comparison between Figs. 4(c) and 4(d), it is speculated that the phase separation is enhanced by the presence of metallic In–Ga. This is because the phase separation is severer at 650 °C than at 700 °C despite the expected lower diffusion mobility of atoms at 650 °C. As discussed above, the annealing in NH_3 flow results in marked phase separation. This result seems to correlate with the existence of metallic In, because, as reported previously, the N-face of InN annealed in NH_3 shows severe degradation.[16,20,21] Hydrogen produced by the decomposition of NH_3 is considered to be responsible for the deterioration and In droplet formation.

By using AlN/Si(111) substrates, as described above, we have clearly observed the phase separation of epitaxial $In_xGa_{1-x}N$ into metallic In–Ga and GaN-rich $In_zGa_{1-z}N$. It should be pointed out that the selection of the substrate and/or interlayer for InGaN growth is also a critical issue in the observation of such phase separation. If a GaN template or a GaN buffer is used, as in many cases,[11–14] the peak for GaN-rich $In_zGa_{1-z}N(0002)$ is difficult to separate from the peak for the GaN(0002) template or buffer because the InN content in $In_zGa_{1-z}N$ is very small (~0.03). For example, we would not notice the phase separation if the films are grown on GaN templates at approximately 700 °C, as expected from the result shown in Fig. 4(c). The InN content in epitaxial InGaN is also an important factor in the observation of phase separation. When InGaN with a higher InN content is selected so that it has a diffraction peak at $2\theta \sim 33°$, it is difficult to distinguish its peak from that of metallic In.

In summary, we have clearly observed the simultaneous formation of metallic In–Ga and GaN-rich InGaN during the MOVPE growth of $In_xGa_{1-x}N$ ($x \sim 0.3$) at 650 °C, as a result of phase separation. The simultaneous emergence of both the metallic In–Ga and GaN-rich InGaN is accompanied by the consumption of the epitaxial $In_xGa_{1-x}N$ ($x \sim 0.3$). Metallic In–Ga is formed through the InN-rich InGaN owing to the thermal instability of InN-rich InGaN. These findings clearly show that $In_xGa_{1-x}N$ ($x \sim 0.3$) is phase-separated into InN-rich InGaN and GaN-rich InGaN. The annealing of the sample in NH_3 flow at 650 °C is found to markedly enhance the decomposition reaction. The decomposition reaction is found to be suppressed by reducing the growth temperature to 570 °C. Such a clear observation of phase separation of InGaN was made possible by the use of AlN/Si(111) substrates.

Acknowledgment This work was supported in part by the "Creative research for clean energy generation using solar energy" project in Core Research for Evolutional Science and Technology (CREST) programs of the Japan Science and Technology Agency (JST), Japan.

1) S. Nakamura, T. Mukai, and M. Senoh, J. Appl. Phys. **76**, 8189 (1994).
2) S. Nakamura, M. Senoh, N. Iwasa, S. Nagahama, T. Yamada, and T. Mukai, Jpn. J. Appl. Phys. **34**, L1332 (1995).
3) A. G. Bhuiyan, K. Sugita, A. Hashimoto, and A. Yamamoto, IEEE J. Photovoltaics **2**, 276 (2012).
4) I. Ho and G. B. Stringfellow, Appl. Phys. Lett. **69**, 2701 (1996).
5) T. Sugahara, M. Hao, T. Wang, D. Nakagawa, Y. Naoi, K. Nishino, and S. Sakai, Jpn. J. Appl. Phys. **37**, L1195 (1998).
6) B. V. Daele, G. V. Tendeloo, K. Jacobs, I. Moerman, and M. R. Leys, Appl. Phys. Lett. **85**, 4379 (2004).
7) J. Kim, H. Kim, and S.-N. Lee, Curr. Appl. Phys. **11** [4], S167 (2011).
8) Z. Li, J. Liu, M. Feng, K. Zhou, S. Zhang, H. Wang, D. Li, L. Zhang, D. Zhao, D. Jiang, H. Wang, and H. Yang, Appl. Phys. Lett. **103**, 152109 (2013).
9) K. Osamura, S. Naka, and Y. Murakami, J. Appl. Phys. **46**, 3432 (1975).
10) T. Matsuoka, N. Yoshimoto, T. Sasaki, and A. Katsui, J. Electron. Mater. **21**, 157 (1992).
11) N. A. El-Masry, E. L. Piner, S. X. Liu, and S. M. Bedair, Appl. Phys. Lett. **72**, 40 (1998).
12) D. Doppalapudi, S. N. Basu, K. F. Ludwig, Jr., and T. D. Moustakas, J. Appl. Phys. **84**, 1389 (1998).
13) B. N. Pantha, J. Li, J. Y. Lin, and H. X. Jiang, Appl. Phys. Lett. **96**, 232105 (2010).
14) Ö. Tuna, W. M. Linhart, E. V. Lutsenko, M. V. Rzheutski, G. P. Yablonskii, T. D. Veal, C. F. McConville, C. Giesen, H. Kalisch, A. Vescan, and M. Heuken, J. Cryst. Growth **358**, 51 (2012).
15) J. W. Ho, L. Zhang, Q. Wee, A. A. O. Tay, M. Heuken, and S.-J. Chua, J. Cryst. Growth **383**, 1 (2013).
16) K. Sugita, A. Hashimoto, and A. Yamamoto, Phys. Status Solidi C **6**, S393 (2009).
17) W. J. Wang, H. Miwa, A. Hashimoto, and A. Yamamoto, Phys. Status Solidi C **3**, 1519 (2006).
18) S. Yu. Karpov, MRS Internet J. Nitride Semicond. Res. **3**, 16 (1999).
19) A. Yamamoto, A. Mihara, Y. Zheng, and N. Shigekawa, Jpn. J. Appl. Phys. **52**, 08JB19 (2013).
20) H. Miwa, A. Hashimoto, and A. Yamamoto, Phys. Status Solidi C **3**, 1536 (2006).
21) A. Yamamoto, K. Sugita, Y. Nagai, and A. Hashimoto, Phys. Status Solidi C **5**, 1762 (2008).